RESEARCH ARTICLE

RSP Science Hub

International Research Journal on Advanced Science Hub
2582-4376
www.rspsciencehub.com
Vol. 07, Issue 05 May

Check for updates

http://dx.doi.org/10.47392/IRJASH.2025.050

Exploring the Structural, Surface Morphological and Magnetic Properties of Eu Doped MnFeO3 Nanomaterials

Dipak Nath[1], A. Robert Xavier[2], Supoto Rhakho[3]

[1]Research Scholar, Department of Physics, St. Joseph University, Chumoukedima.Nagaland, India

[1]Associate Professor, Department of Physics, Kohima Science College Jotsoma, Kohima, Nagaland, India

[2]Professor, Department of Physics, St. Joseph University, Chumoukedima, Nagaland, India

[3]Postgraduate Student, Department of Physics, Kohima Science College Jotsoma, Kohima, Nagaland, India

Emails: *dipaknath03081976@gmail.com[1], arobertxavier@gmail.com[2], supotorhakho@gmail.com[3]*

Article History

Received: 04 April 2025
Accepted: 22 April 2025
Published: 07 May 2025

Keywords:
Europium doped $MnFeO_3$ perovskite; Field emission scanning electron microscopy; Magnetic characterization; Solution combustion synthesis; X-ray diffraction.

Abstract

This study explores the impact of Europium (Eu) doping on the structural, morphological, and magnetic properties of manganese ferrite perovskite ($MnFeO_3$), a material with significant potential for advanced technological applications. $MnFeO_3$ was synthesized using the solution combustion method, an energy-efficient technique that enables the production of fine powders with controlled purity and morphology. X-ray diffraction (XRD) analysis confirmed the formation of a spinel cubic perovskite structure. A noticeable decrease in crystallinity was observed with increasing Eu doping concentrations (0%, 5%, and 9%), suggesting lattice distortion without altering the overall phase structure. Field emission scanning electron microscopy (FESEM) revealed a reduction in particle size and notable changes in surface morphology with higher Eu content. Energy dispersive X-ray (EDX) spectroscopy confirmed the successful incorporation of Eu into the $MnFeO_3$ lattice, as evidenced by the presence of Mn, Fe, O, and Eu peaks. Magnetic measurements conducted using vibrating sample magnetometry (VSM) showed that Eu doping significantly influenced the magnetic properties of $MnFeO_3$, leading to variations in both saturation magnetization and coercivity. Overall, the findings demonstrate that Eu doping is an effective approach for tuning the structural, morphological, and magnetic characteristics of $MnFeO_3$ for advanced functional applications.

1. Introduction

Manganese ferrite oxide ($MnFeO_3$) has emerged as a promising perovskite oxide due to its compelling magnetic, electrical, and photocatalytic properties. These multifunctional characteristics make it a strong candidate for various advanced technologies, including magnetic sensing, data storage, catalysis, and especially spintronic applications. Spintronics, which exploits the spin of electrons in addition to their charge, requires materials with tuneable magnetic ordering, high spin polarization, and structural stability. A widely explored approach to achieving such enhancements in perovskite systems is the substitution of host cations with rare-earth elements, which can significantly modify their

structural and magnetic behaviour (Alahmari & Fatima, 2024). In this context, europium (Eu) has been selected as a dopant for $MnFeO_3$ due to its unique $4f^6$ electronic configuration, redox flexibility, and strong spin-orbit coupling, all of which influence the magnetic exchange interactions and spin alignment in the host lattice. Europium belongs to the lanthanide series and is known for its high reactivity, soft metallic nature, and characteristic red photoluminescence. Its ability to exist in both +2 and +3 oxidation states enable dynamic control over charge compensation, defect formation, and valence state modulation—factors that are critically important in tailoring the magnetic and electronic properties required for spintronic devices. $MnFeO_3$ typically crystallizes in an orthorhombic $GdFeO_3$-type perovskite structure (ABO_3), where Mn^{3+} occupies the A-site and Fe^{3+} the B-site. The substitution of Mn^{3+} with the larger Eu^{3+} ion induces local lattice strain and distortions due to ionic size mismatch, altering bond angles and magnetic superexchange pathways. These changes can enhance ferromagnetic ordering, reduce magnetic frustration, and promote spin coherence. In this study, Eu-doped $MnFeO_3$ nanomaterials were synthesized via the solution combustion method and sintered at 400 °C and 800 °C to investigate the role of thermal treatment in property optimization (Nguyen et al., 2021). X-ray diffraction (XRD) confirmed the retention of the orthorhombic perovskite phase, with reduced crystallite size upon doping (Sain et al., 2014). Field Emission Scanning Electron Microscopy (FESEM) revealed improved surface homogeneity, while Vibrating Sample Magnetometry (VSM) showed enhanced magnetic response, attributed to Eu-induced structural and electronic modifications. (Saeidi et al., 2023) This work aims to explore the effects of Eu substitution on the structural, morphological, and magnetic properties of $MnFeO_3$ nanomaterials, emphasizing their potential for next-generation spintronic applications.

2. Literature Review

Manganese ferrite ($MnFeO_3$), a perovskite-type transition metal oxide, has garnered considerable attention due to its multifunctional properties including magnetism, photocatalysis, and electrical conductivity. These characteristics make it a candidate for applications in magnetic storage, environmental remediation, and spintronic devices. A widely explored strategy to modulate these properties involves doping with rare-earth ions such as europium (Eu^{3+}), which can induce structural distortions and alter magnetic exchange interactions due to its unique electronic configuration Structural characterization of such doped nanomaterials commonly employs X-ray diffraction (XRD). One of the most widely used models for estimating crystallite size from XRD peak broadening is the Debye–Scherrer equation, formulated as:

$$D = \frac{K\lambda}{\beta\cos\theta}$$

where D is the average crystallite size, λ is the X-ray wavelength, β is the full width at half maximum (FWHM) of the diffraction peak in radians, θ is the Bragg angle, and K is the shape factor (typically ~0.9). This method, originally introduced by Paul Scherrer and often referred to as the Scherrer or Debye–Scherrer equation, remains a fundamental tool in nanoscale material analysis (Holzwarth et al., 2011). Recent studies highlight the significance of Eu^{3+} doping in tailoring the structural and magnetic properties of Mn-based ferrites. Saeidi et al. (2023) synthesized Eu-substituted Mn–Zn ferrite nanoparticles via co-precipitation and hydrothermal routes. XRD analysis showed a reduction in crystallite size upon Eu incorporation, attributed to lattice distortion from the larger ionic radius of Eu^{3+} compared to Mn^{2+}/Fe^{3+}. Additionally, a decrease in magnetic saturation with increasing Eu content was reported, due to the disruption of Fe^{3+}–O–Fe^{3+} super exchange pathways. Photoluminescence and optical tuning upon Eu doping have also been observed in similar oxide systems. For instance, Bhat et al. (2024) investigated Eu^{3+}-doped $SrSnO_3$ perovskites and found strong emission at 612 nm attributed to the $^5D_0 \rightarrow {}^7F_2$ transition. The optimized doping concentration (5 mol%) yielded maximum luminescence, while higher concentrations resulted in quenching effects consistent with the Blasse model. Surface morphological studies using FESEM and AFM across various doped oxide nanomaterials reveal that Eu doping can improve homogeneity and reduce porosity, resulting in smoother surfaces and enhanced photocatalytic potential. Achille et al. (2021) further demonstrated that Eu^{3+} doping in CeO_2 nanocubes improved fluorescence intensity, whereas increased structural defects in other morphologies led to diminished emission, indicating the critical role of crystal symmetry and defect control. Magnetic characterization, typically performed via Vibrating

Sample Magnetometry (VSM), shows that Eu^{3+} incorporation into the $MnFeO_3$ lattice enhances ferromagnetic interactions through modified bond angles and altered cation distributions. The unpaired 4f electrons of Eu^{3+} may also contribute to magnetic ordering indirectly by influencing lattice strain and oxygen vacancy formation. In parallel, compositional, and morphological tuning using other dopants such as Nb has also shown promising improvements in $MnFeO_3$ systems. Alahmari et al. (2024) reported enhanced oxygen evolution reaction (OER) activity in Nb-doped $MnFeO_3$ due to increased surface area, reduced charge transfer resistance, and better OH^- adsorption capability, highlighting the catalytic versatility of doped perovskites. These findings underscore that Eu^{3+} doping is a viable strategy for enhancing the structural, morphological, and magnetic properties of $MnFeO_3$ nanomaterials, with implications for multifunctional applications in catalysis, spintronics, and biomedical imaging.

3. Methodology

3.1. Synthesis of Europium-Doped Perovskite Manganese Ferrite (Eu-Doped $MnFeO_3$) via Solution Combustion Method

Perovskite-type manganese ferrite ($MnFeO_3$) is known for its excellent electronic, magnetic, and catalytic properties, which can be further enhanced by doping with rare-earth ions such as europium (Eu^{3+}), making it suitable for applications in spintronics, magnetoelectronic, and photocatalysis. In this study, Eu-doped $MnFeO_3$ nanoparticles were synthesized using the solution combustion synthesis (SCS) method, a rapid, cost-effective, and environmentally friendly approach that offers control over phase purity, stoichiometry, and particle size. Analytical grade manganese nitrate [$Mn(NO_3)_2 \cdot H_2O$], ferric nitrate [$Fe(NO_3)_3 \cdot 9H_2O$], europium nitrate [$Eu(NO_3)_3 \cdot 6H_2O$], and fuels such as urea or glycine were used without further purification. The metal precursors were dissolved in deionized water and mixed with fuel based on redox balance, then stirred to form a clear homogeneous solution. This solution was transferred to a preheated muffle furnace (300–600 °C), where it underwent a self-sustaining combustion reaction, yielding a voluminous ash-like nanopowder. The resulting powder was ground and calcined in air at 400–800 °C for 2–4 hours to improve crystallinity and eliminate residual organics.

3.2. Characterization Techniques

The characterization of Eu-doped $MnFeO_3$ nanomaterials was performed using multiple techniques. XRD was employed to analyze the crystallographic structure and crystallite size, while FESEM and EDX provided information on surface morphology and elemental composition. The magnetic properties were investigated using VSM. The flow chart of characterizing Eu Doped $MnFeO_3$ Nanomaterials is shown in fig 1

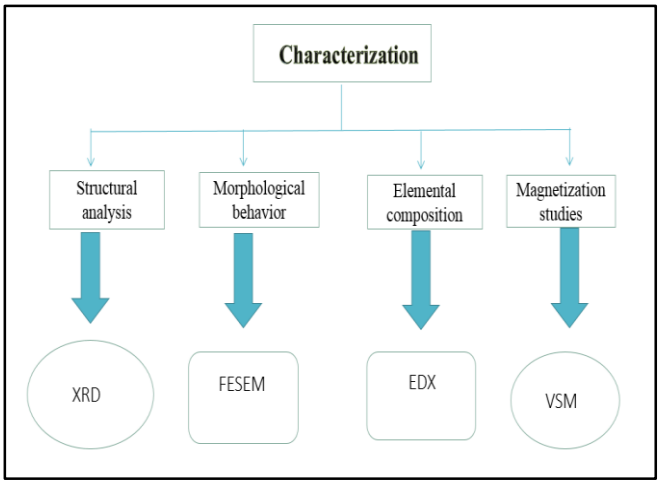

Figure 1 Flow Chart of Characterizing Eu Doped MnFeO3 Nanomaterials

3.3. X-ray Diffraction (XRD)

X-ray Diffraction (XRD) analysis was employed to investigate the crystal structure, phase purity, lattice parameters, degree of crystallinity, and average crystallite size of the synthesized Eu-doped $MnFeO_3$ nanomaterials. The measurements were performed using a diffractometer equipped with Cu-Kα radiation (λ = 1.5404 Å). The diffraction patterns were recorded in the 2θ range of [insert scan range, e.g., 10°–80°], with an appropriate step size and scan rate to ensure high-resolution data. (Sindhu et al., 2024). The interaction of monochromatic X-rays with the atomic planes of the crystalline samples produced characteristic diffraction patterns based on Bragg's law (Fig 2), allowing for the identification of crystallographic phases and structural parameters. Due to the wave-like nature of X-rays and their comparable wavelength to interatomic distances, constructive interference occurs at specific angles, reflecting the material's internal atomic arrangement (Balta & Simsuk, 2022).

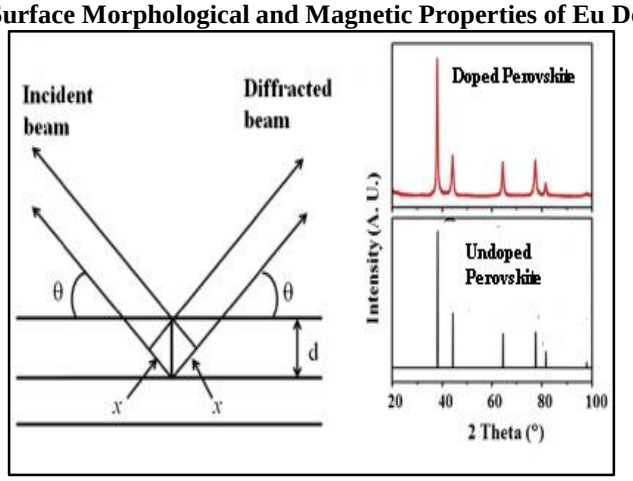

Figure 2 Principle of XRD Along with Virtual Graph

Paul Scherrer was among the first to study the influence of limited particle size on diffraction broadening. This led to the formulation of the well-known Scherrer equation, which relates peak broadening to crystallite size and is expressed as:

$$D = \frac{K\lambda}{\beta \cos\theta}$$

where **D** is the crystallite size (nm), **K** is the Scherrer constant (typically 0.9), **λ** is the X-ray wavelength (1.5404 Å for Cu-Kα), **β** is the full width at half maximum (FWHM) in radians, and **θ** is the Bragg angle. A diffraction pattern was obtained by plotting the X-ray intensity against the diffraction angle (2θ), as illustrated in **Fig. 2**. This analysis is crucial for identifying the crystal structure of the material, as the position and intensity of the diffraction peaks correspond to specific crystallographic planes. By comparing the observed pattern with standard reference data, the phase composition and symmetry of the Eu-doped $MnFeO_3$ nanomaterials can be determined, confirming the formation of a crystalline perovskite structure.

3.4. Field Emission Scanning Electron Microscopy (FESEM)

The Schematic diagram of Field Emission Scanning Electron Microscope (FESEM) is shown in Fig 3. It is employed to examine the surface morphology, particle size, and microstructure of nanomaterials at high resolution. FESEM works by emitting a finely focused beam of high-energy electrons onto the sample surface. The interaction between the incident electrons and the sample atoms generates secondary and backscattered electrons, which are detected to form a high-resolution image (Achille et al., 2021).

Because FESEM requires a conductive surface, non-conductive samples are coated with a thin layer of gold. The emitted secondary electrons, typically with energies between 3–5 eV, provide detailed information about the topography, surface roughness, and particle distribution at the nanoscale.

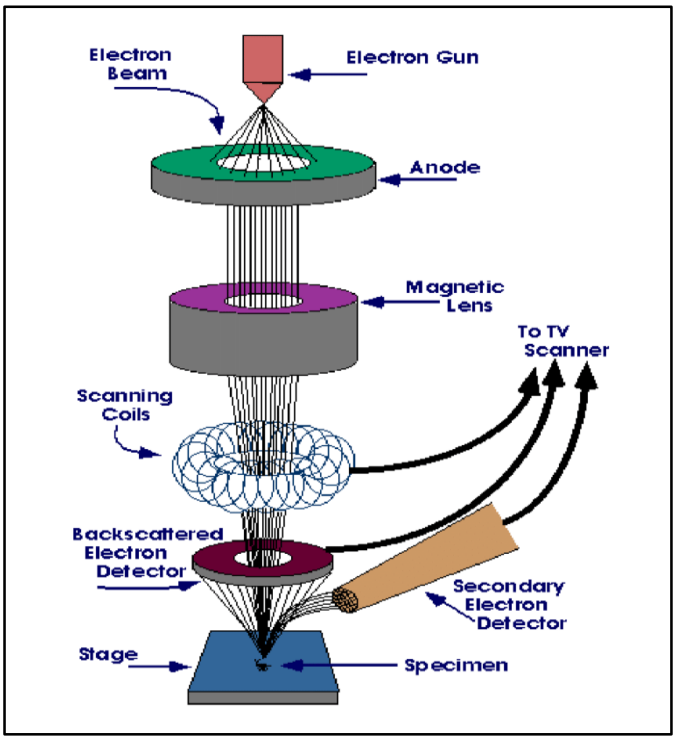

Figure 3 Schematic diagram of Field Emission Scanning Electron Microscope. Source: Areef Billah (2016)

3.5. Energy Dispersive X-ray Spectroscopy (EDX)

Energy Dispersive X-ray Spectroscopy (EDX), often used in combination with FESEM, is a qualitative and semi-quantitative tool used to analyze the elemental composition of materials (Fig 4). When the electron beam interacts with the atoms in the sample, inner-shell electrons are ejected, and higher-energy electrons fall into the vacant states, emitting X-rays characteristic of each element. The energy and intensity of these emitted X-rays are recorded to identify and quantify the elements present. This technique helps confirm the successful doping of europium (Eu^{3+}) into the $MnFeO_3$ lattice and assess sample purity and elemental homogeneity. The spectral peaks (e.g., Kα, Lα) are described using Siegbahn notation, providing detailed atomic-level compositional information.

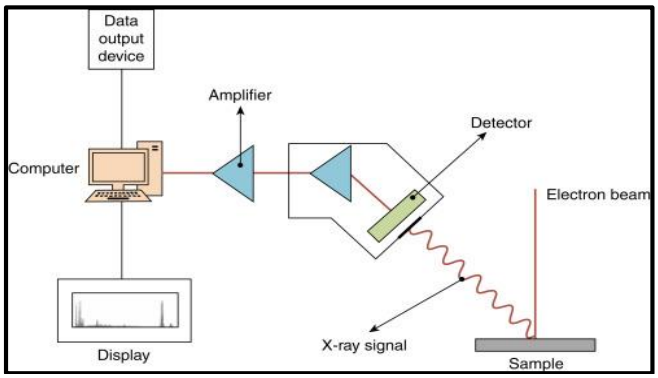

Figure 4 Energy Dispersive X-ray Spectroscopy Analysis- an overview (Source:https://www.sciencedirect.com/topics/engineering/energy-dispersive-x-ray-spectroscopy-analysis)

3.6. Vibrating Sample Magnetometry (VSM)

The Schematic diagram of Vibration Sample Magnetometer (VSM) is shown in Fig 5. It is used to characterize the magnetic properties of Eu-doped $MnFeO_3$ nanomaterials (Niazi et al., 2000). It operates on Faraday's Law of Electromagnetic Induction. In VSM, the sample is vibrated sinusoidally within a uniform magnetic field, inducing a change in magnetic flux detected by surrounding pickup coils (Singh et al., 2008). The induced voltage is directly proportional to the sample's magnetization. The output is recorded as a magnetization (M) versus applied field (H) hysteresis loop, which reveals crucial magnetic parameters such as saturation magnetization (M), coercivity (Hc), and remanence (Mr). These parameters are essential for evaluating the influence of Eu doping on the magnetic behavior of the $MnFeO_3$ nanomaterial and its suitability for spintronic or magnetic storage applications.

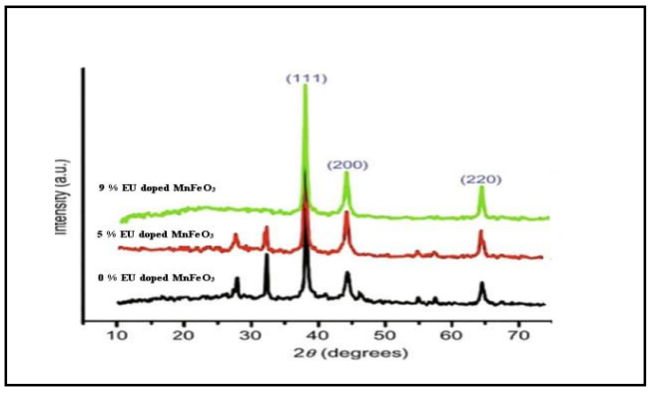

Figure 5 Schematic Diagram of Vibration Sample Magnetometer (Source: www.cet-science.com)

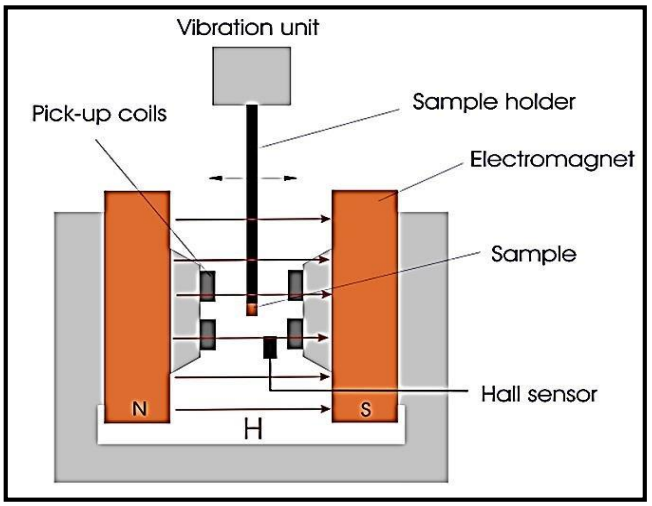

Figure 6 XRD Patterns of Unhoped and doped MnFeO3

4. Results and Discussion

4.1. Structural Analysis

The crystallographic structure and crystallite sizes of undoped and europium (Eu)-doped $MnFeO_3$ nanomaterials were examined using X-ray diffraction (XRD). The PXRD patterns of the as-formed and Eu-doped (5 and 9 at.%) $MnFeO_3$ samples revealed three predominant peaks corresponding to the (111), (200), and (220) planes, as shown in **Fig. 6.** These diffraction peaks match well with the standard JCPDS data, confirming the formation of an orthorhombic perovskite structure. No secondary phases or impurity peaks were detected, indicating the successful substitution of Eu^{3+} ions into the $MnFeO_3$ lattice without altering the host phase. The intensity and slight shifts in the peak positions with increasing Eu concentration suggest changes in lattice strain and slight modification of the unit cell dimensions due to ionic size mismatch between Eu^{3+} and Mn^{3+}/Fe^{3+} ions. The crystallite size was estimated using the Scherrer equation, indicating nanoscale dimensions that slightly decreased with higher Eu doping levels, consistent with the peak broadening observed in the diffractograms. The crystallite size and average crystallite size were calculated using the Debye–Scherrer formula, as detailed below.

$$D = \frac{K\lambda}{\beta \cos\theta}$$

Where K = Shape factor = 0.9

λ = X-ray wavelength = 1.5406 Å (For Cu Kα)

Table 1 0% Eu doped $MnFeO_3$

Plane (hkl)	2θ (°)	θ (rad)	FWHM (°)	FWHM (rad) β	cos(θ)	Crystallite Size (nm)
(111)	38.25	0.33	0.25	0.0043	0.99	31.77
(200)	44.56	0.38	0.30	0.0052	0.99	26.48
(220)	65.203	0.56	0.35	0.0061	0.99	22.69

The average crystallite size of $MnFeO_3$ doped with 0% Eu is 26.98 nm.

Table 2 5% Eu doped $MnFeO_3$

Plane (hkl)	2θ (°)	θ (rad)	FWHM (°)	FWHM (rad) β	cos(θ)	Crystallite Size (nm)
(111)	38.25	0.33	0.28	0.0048	0.99	28.37
(200)	44.56	0.38	0.34	0.0059	0.99	23.36
(220)	65.20	0.56	0.38	0.0066	0.99	20.90

The average crystallite size of $MnFeO_3$ doped with 5% Eu is 24.21 nm.

Table 3 9% Eu doped $MnFeO_3$

Plane (hkl)	2θ (°)	θ (rad)	FWHM (°)	FWHM (rad) β	cos(θ)	Crystallite Size (nm)
(111)	38.25	0.33	0.32	0.0055	0.99	24.82
(200)	44.56	0.38	0.39	0.0068	0.99	20.37
(220)	65.20	0.56	0.44	0.0076	0.99	18.05

The average crystallite size of $MnFeO_3$ doped with 9% Eu is 21.08 nm.

Analysis was conducted on the major diffraction planes (111), (200), and (220) to determine average crystallite sizes. For the undoped $MnFeO_3$ (0% Eu), the average crystallite size was approximately 26.99 nm. Upon doping with 5% Eu, the size reduced to 24.22 nm, and further decreased to 21.08 nm at 9% Eu doping. This consistent and gradual decrease in crystallite size indicates that the incorporation of Eu^{3+} ions effectively inhibit the grain growth during the combustion synthesis process. The dopant likely acts as a barrier at grain boundaries, impeding particle coalescence and resulting in finer crystallites. The decrease in crystallite size leads to a notable increase in the surface-to-volume ratio, which significantly influences the material's physical and chemical behaviour. A larger surface area relative to volume enhances surface reactivity and can improve interactions with magnetic fields or catalytic environments. This structural refinement may therefore contribute to improved magnetic behaviour, as observed in related VSM measurements. Moreover, the broadening of the diffraction peaks in the XRD pattern with increased Eu content further supports the reduction in crystallite size. Peak broadening is typically attributed to both size effects and lattice strain; however, in this study, the trend in size reduction across all three crystallographic planes (111), (200), and (220) suggests that the effect is predominantly due to particle size refinement rather than anisotropic strain. Additionally, the absence of secondary phases in all samples confirms the successful incorporation of Eu ions into the $MnFeO_3$ perovskite lattice without disrupting the overall crystal structure. The single-phase orthorhombic structure is retained across all doping levels, demonstrating the structural stability of the system under Eu substitution. In summary, the XRD analysis verifies the formation of single-phase, orthorhombic $MnFeO_3$ in both doped and undoped forms. Europium doping leads to a systematic reduction in crystallite size, a more refined and homogeneous microstructure, and potentially enhanced functional properties due to increased surface area and improved structural uniformity.

4.2. Morphology Analysis

Fig 7 shows the FESEM images along with the corresponding Energy Dispersive X-ray (EDX) spectra.

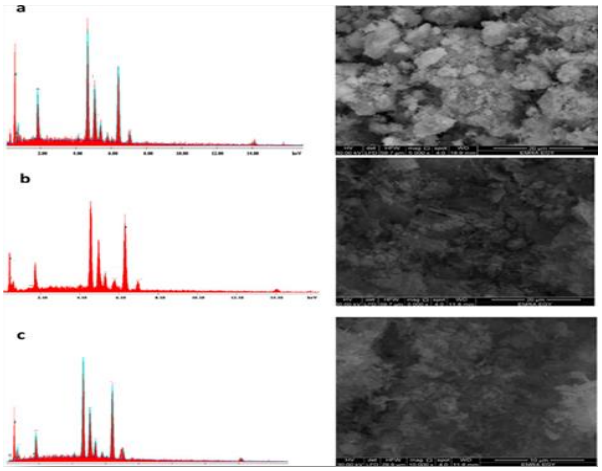

Figure 7 EDX (Left) & FESEM (Right)

4.3. Energy-Dispersive X-ray Spectroscopy (EDX) Analysis

Energy-dispersive X-ray spectroscopy (EDX) was employed to determine the elemental composition of the synthesized samples, corresponding to the spectra labelled (a), (b), and (c) in Fig 7. The EDX spectra confirmed the presence of manganese (Mn), iron (Fe), and oxygen (O) as the major constituents in all samples, consistent with the $MnFeO_3$ composition. In addition, europium (Eu) peaks were clearly detected in the doped samples, verifying successful incorporation of the dopant into the host matrix. All spectra exhibited dominant peaks corresponding to Mn and Fe, along with characteristic oxygen peaks. In samples (b) and (c), the presence of Eu was confirmed by minor but distinct peaks, indicating successful doping without the formation of secondary phases, as no unexpected elements or phase-specific signals were observed. This supports the XRD findings, which revealed a single-phase perovskite structure.

- **Sample (a)** (undoped $MnFeO_3$) displayed sharp, well-defined peaks with high intensity, confirming the high purity and successful formation of the base material. The corresponding SEM image showed uniform particle dispersion, correlating with the homogeneous elemental distribution observed in the EDX spectrum.
- **Sample (b)** (5% Eu-doped $MnFeO_3$) exhibited slightly lower Mn and Fe peak intensities compared to sample (a), accompanied by the emergence of weak Eu peaks. This shift reflects the substitution of Mn or Fe atoms by Eu ions and the slight reduction in base metal content. The SEM image for this sample indicated mild agglomeration, possibly influencing the local concentration and detectability of elements during EDX scanning.
- **Sample (c)** (9% Eu-doped $MnFeO_3$) showed more pronounced Eu peaks but comparatively lower Mn and Fe intensities. The overall peak intensity reduction could be linked to increased particle aggregation and denser surface morphology, as seen in the SEM images. These features can limit the effective X-ray generation and detection due to shielding effects or reduced surface exposure.

The increase in Eu content across the doped samples corresponds to a slight elemental substitution within the crystal lattice, which appears to affect both structural compactness and microstructure uniformity. Importantly, no impurity peaks were detected, indicating phase stability and high chemical homogeneity even at higher Eu concentrations. In conclusion, the EDX analysis verifies the elemental composition and successful doping of Eu into $MnFeO_3$. The progressive change in elemental peak profiles with increasing Eu content not only confirms effective dopant incorporation but also reflects subtle changes in surface structure and particle agglomeration, which can further influence magnetic and catalytic properties.

4.4. Field Emission Scanning Electron Microscopy (FESEM) Analysis

FESEM analysis was carried out to investigate the surface morphology and microstructural evolution of Eu-doped $MnFeO_3$ nanomaterials. The micrographs of samples (a), (b), and (c) in Fig 7, corresponding to 0%, 5%, and 9% Eu doping, respectively, reveal significant changes in morphology with increasing dopant concentration.

- **Sample (a)** (0% Eu, undoped $MnFeO_3$) exhibits a highly porous structure composed of irregularly shaped, loosely connected particles with noticeable agglomeration. The morphology reflects the rapid gas evolution typical of the solution combustion synthesis (SCS) process, which often produces foam-like structures. The grains are non-uniform and poorly connected, indicating limited control over particle nucleation and growth. This morphology is

indicative of high surface energy and incomplete crystallization, leading to structural instability and uneven grain distribution.

- **Sample (b)** (5% Eu doping) shows a more refined and uniform microstructure. The particles exhibit reduced agglomeration and a more porous, flake-like or foam-like texture, with some regions appearing fragmented into finer particles. This suggests that the introduction of Eu^{3+} ions play a role in moderating grain growth, leading to improved particle dispersion. The reduction in particle size and the more open, porous framework are likely due to the dopant's influence on reaction kinetics and energy release during combustion, which promotes finer nucleation and inhibits uncontrolled grain coalescence.
- **Sample (c)** (9% Eu doping) reveals further refinement of the morphology. The particles appear even smaller and exhibit increased porosity. The structure consists of irregular, nanosheet-like formations with finer features. However, evidence of secondary agglomeration is observed, which is common in nanoparticles due to their high surface energy. Despite this, the overall morphology is more homogeneous and suggests enhanced surface-to-volume ratios, which can significantly impact the material's surface reactivity and functional properties.

Overall, the FESEM results demonstrate that increasing Eu content leads to improved structural uniformity, finer particle sizes, and enhanced porosity. Europium doping effectively suppresses excessive grain growth during synthesis and promotes the formation of more reactive, nanostructured surfaces. These morphological changes are expected to have a direct influence on the material's magnetic, catalytic, and electronic behaviour.

4.5. Magnetic Properties

The magnetic properties of undoped and Eu-doped $MnFeO_3$ samples sintered at 400 °C and 800 °C were studied using vibrating sample magnetometer (VSM) measurements, as shown in the M–H curves (Fig. 8). Hysteresis loops recorded at room temperature revealed changes in saturation magnetization (M_s), remanence (M_r), and coercivity (Hc). Eu doping and higher sintering temperatures influenced magnetic ordering, with Eu^{3+} ions slightly weakening magnetic interactions due to their non-magnetic nature. The results confirm that Eu substitution effectively tunes the magnetic behavior of $MnFeO_3$ nanomaterials. The variation in magnetic parameters highlights the role of microstructural evolution during doping and thermal treatment. These findings are crucial for optimizing such materials for spintronic and magnetic device applications.

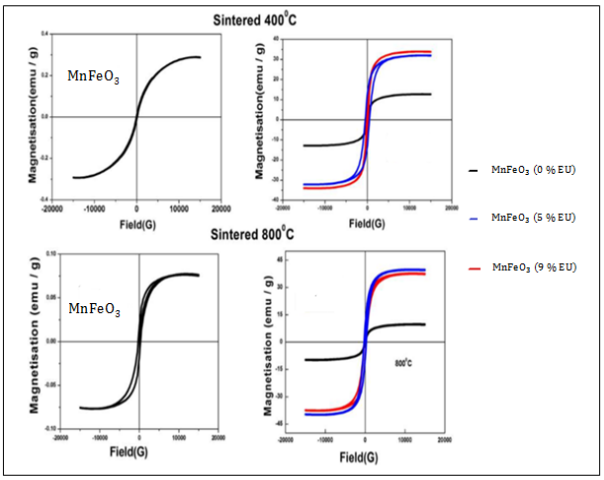

Figure 8 MH Curves at 400 °C & 800 °C

At 400 °C, the undoped $MnFeO_3$ sample exhibits a narrow hysteresis loop, indicative of weak ferromagnetism. The low values of saturation magnetization (Ms), coercivity (Hc), and remanence (Mr) suggest the material retains a largely antiferromagnetic character, with minor spin canting contributing to the weak ferromagnetic response. With europium doping at 5% and 9%, a noticeable enhancement in magnetic behaviour is observed. The hysteresis loops become broader, indicating increased ferromagnetic ordering. In particular, the 9% Eu-doped sample exhibits the highest Ms value, signifying the development of uncompensated spins and strengthened magnetic exchange interactions. This suggests that even at lower sintering temperatures, Eu^{3+} ions influence the magnetic microstructure, possibly by modifying local exchange pathways and disrupting antiferromagnetic alignment. Samples sintered at 800 °C show similar trends but with improved magnetic properties overall. The undoped $MnFeO_3$ sample still exhibits weak ferromagnetism, but with

a slightly higher Ms than its 400 °C counterpart, attributed to enhanced crystallinity and grain growth. Eu-doped samples demonstrate a substantial increase in magnetization, with broader and more pronounced hysteresis loops. The 9% Eu-doped sample again shows the highest Ms, but with a more significant enhancement than at 400 °C. This improvement is likely due to reduced structural defects and improved crystallite connectivity at the higher sintering temperature, which facilitate stronger magnetic exchange interactions. Overall, the combination of europium doping, and elevated sintering temperature synergistically enhances the magnetic properties of $MnFeO_3$, demonstrating the effectiveness of these parameters in tailoring the material's magnetic performance for advanced functional applications.

Conclusion

In this study, europium doped $MnFeO_3$ nanocrystals were successfully synthesized using the solution combustion method, followed by sintering at 400 °C and 800 °C. Powder X-ray diffraction (XRD) confirmed the formation of a single-phase orthorhombic perovskite structure with high phase purity across all samples. Field Emission Scanning Electron Microscopy (FESEM) revealed uniformly distributed, agglomerated nanoparticles. A reduction in particle size with increasing Eu content was observed, indicating that europium incorporation effectively inhibits grain growth during synthesis. Elemental analysis using Energy-Dispersive X-ray Spectroscopy (EDX) verified the presence of Mn, Fe, O, and Eu, confirming successful substitutional doping. Magnetic characterization using a vibrating sample magnetometer (VSM) demonstrated that all samples exhibit weak ferromagnetic behavior, with noticeable enhancement in magnetization as Eu doping increased. This improvement is attributed to modified magnetic exchange interactions and the formation of oxygen vacancies induced by Eu^{3+} substitution. Overall, the incorporation of europium not only tailors the structural and morphological features of $MnFeO_3$ nanocrystals but also significantly enhances their magnetic properties. These results suggest that Eu-doped $MnFeO_3$ is a promising candidate for future applications in spintronic devices and magnetic materials.

Acknowledgements

The authors, gratefully thank to Kohima Science College Jotsoma, Nagaland & St Joseph University, Nagaland for support & help while writing this article.

References

[1]. Achille, A., Anne, E. D., Wallace, R. M., & Coffer, J. C. (2021). Morphology-dependent fluorescence of europium-doped cerium oxide nanomaterials. Nanoscale Advances, 3(13), 3563–3572.

[2]. Alahmari, A. A., Khan, M., Ahamad, T., & Alshehri, S. M. (2024). Nb-doped $MnFeO_3$ as a high-performance electrocatalyst for oxygen evolution reaction. Journal of Alloys and Compounds, 940, 168946. https://doi.org/10.1016/j.jallcom.2023.168946.

[3]. Alahmari, S. D., & Fatima, A. (2024). Improvement in electrochemical performance of $MnFeO_3$ using Nb-doping strategy for oxygen evolution reaction. The European Physical Journal Plus, 139(12). http://dx.doi.org/10.1140/epjp/s13360-024-05868-8

[4]. Balta, Z., & Simsuk, E. B. (2022). Understanding the structural and photocatalytic effects of incorporation of hexagonal boron nitride whiskers into ferrite-type perovskites ($BiFeO_3$, $MnFeO_3$) for effective removal of pharmaceuticals from real wastewater. Journal of Alloys and Compounds, 898. https://doi.org/10.1016/j.jallcom.2021.162897

[5]. Bhat, F. A., Qureshi, M. M., & Reshi, B. I. (2024). Structural and photoluminescence properties of Eu^{3+} doped $SrSnO_3$ perovskite phosphors for optoelectronic applications. Materials Today Communications, 38, 107293. https://doi.org/10.1016/j.mtcomm.2024.107293.

[6]. Brozek-Mucha, Z. (2007). Comparison of cartridge case and airborne GSR—a study of the elemental composition and morphology by means of SEM-EDX. X-Ray Spectrometry.

[7]. Fatimah, S., et al. (2022). How to calculate crystallite size from X-ray (XRD) using Scherrer method. ASEAN Journal of Science and Engineering.

[8]. Field Emission Scanning Electron

Microscopy. (n.d.). Retrieved from https://www.sciencedirect.com.

[9]. Gaston, K., & Protter, N. (2019). Energy-dispersive X-ray spectroscopy (EDX). Spectroscopy.

[10]. Holzwarth, U., & Gibson, N. (2011). The Scherrer equation versus the 'Debye-Scherrer equation'. Nature Nanotechnology.

[11]. Holzwarth, U., & Gibson, N. (2011). The Scherrer equation versus the 'Debye-Scherrer equation'. Nature Nanotechnology, 6(9), 534. https://doi.org/10.1038/nnano.2011.145.

[12]. Imnatula. (2022). Structural properties of SnO_2. Nanomaterials.

[13]. Khaliq, & Anwar. (2013). Vibrating sample magnetometry: Analysis and construction. 2013.

[14]. Li, Q., Xuan, Y., & Yang, G. (2007). Synthesis and magnetic properties of Mn-Zn ferrite nanoparticles. Journal of Magnetism and Magnetic Materials, 312(2), 464–469. https:// doi.org/ 10.1016 /j.jmmm.2006.11.200

[15]. Mohamed, W., & Abu-Dief, A. M. (2020). Impact of rare earth europium (RE-Eu^{3+}) ions substitution on microstructural, optical and magnetic properties of $CoFe_{2-x}Eu_xO_4$ nanosystems. Ceramics International, 46(10), 15987–15995. https://doi.org/10.1016/j.ceramint.2020.03.175

[16]. Nabi, A., Bi, W., Sofi, S. A., Syed, I. S., Tomar, R., Abd-Rabboh, H. S. M., & Shafi, A. (2024). Europium-doped $SrSnO_3$ perovskite: Structural, spectroscopic, and luminescent characterization for advanced lighting technologies and beyond. Energy & Fuels, 38(24). http://dx.doi.org/10.1021/acs.energyfuels.4c04141

[17]. Nandee, R., Chowdhury, M. A., Hossain, N., Rana, M., Mobarak, M. H., & Khandaker, M. R. (2024). Surface topography and surface morphology of graphene nanocomposite by FESEM, EDX and AFM analysis. Nano-Structures & Nano-Objects, 38(8), 101170. https://doi.org/10.1016/j.nanoso.2024.101170

[18]. Nguyen, T. A., Pham, T. L., Mittova, I. Y., Mittova, V. O., Nguyen, T. L. T., Nguyen, H. V., & Bui, V. X. (2021). Co-doped $NdFeO_3$ nanoparticles: Synthesis, optical, and magnetic properties study. Nanomaterials, 11(4), 937–949.

[19]. Nguyen, T. A., Pham, T. L., Mittova, I. Y., Mittova, V. O., Nguyen, T. L. T., Nguyen, H. V., & Bui, V. X. (2021). Co-doped $NdFeO_3$ nanoparticles: Synthesis, optical, and magnetic properties study. Nanomaterials, 11(4), 937–949.

[20]. Niazi, A., Poddar, P., & Rastogi, K. A. (2000). A precision, low-cost vibrating sample magnetometer. Current Science.

[21]. Saeidi, H., Mozaffari, M., Ilbey, S., Dutz, S., Zahn, D., & Azimi, G. (2023). Effect of europium substitution on the structural, magnetic and relaxivity properties of Mn–Zn ferrite nanoparticles: A dual-mode MRI contrast-agent candidate. Nanomaterials, 13(2), 331. https://doi.org/10.3390/nano13020331

[22]. Saeidi, N., Hadipour, N. L., & Abdolmaleki, A. (2023). Europium-substituted Mn–Zn ferrite nanoparticles for MRI contrast enhancement: Structural and magnetic investigation. Materials Chemistry and Physics, 302, 127668. https://doi.org/10.1016/j.matchemphys.2023.127668.

[23]. Sain, S., Kar, A., Patra, A., & Pradhan, S. K. (2014). Structural interpretation of SnO_2 nanocrystals of different morphologies synthesized by microwave irradiation and hydrothermal methods. CrystEngComm, 16(6), 1079–1088. https://doi.org/10.1039/c3ce42281j

[24]. Sindhu, T., Ravichandran, A. T., Robert Xavier, A., Sofiya, K., & Kumaresavanji, M. (2024). Impact of Gd doping on structural and magnetic characteristics of $SrFeO_3$ perovskite nanomaterial. Journal of Physics: Condensed Matter, 36(50), 505809. https://doi.org/10.1088/1361-648X/ad7b94

[25]. Sing, N. (n.d.). Solid State Physics. Narosa Publishing House.

[26]. Singh, N., Rhee, J. Y., & Auluck, S. (2008). Electronic and magneto-optical properties of rare-earth orthoferrites $RFeO_3$ (R = Y, Sm, Eu, Gd, and Lu). Journal of the Korean Physical Society, 53, 806–811.